Water Resources Research

RESEARCH ARTICLE
10.1029/2019WR025384

Consistent MPFA Discretization for Flow in the Presence of Gravity

M. Starnoni[1], I. Berre[1], E. Keilegavlen[1], and J. M. Nordbotten[1]

[1]Department of Mathematics, University of Bergen, Bergen, Norway

Key Points:
- Standard discretization of two-phase Darcy flow in the presence of gravity is shown to create a persistent unphysical flux field
- We present a new consistent discretization of flow, which treats the gravity term as part of the discrete flux operator
- Our method is generally second-order convergent and is capable of eliminating the flux field arising when using a standard discretization

Correspondence to:
M. Starnoni,
michele.starnoni@uib.no

Citation:
Starnoni, M., Berre, I., Keilegavlen, E., & Nordbotten, J. M. (2019). Consistent mpfa discretization for flow in the presence of gravity. *Water Resources Research*, *55*, 10,105–10,118. https://doi.org/10.1029/2019WR025384

Received 11 APR 2019
Accepted 10 NOV 2019
Accepted article online 16 NOV 2019
Published online 3 DEC 2019

©2019. The Authors.
This is an open access article under the terms of the Creative Commons Attribution License, which permits use, distribution and reproduction in any medium, provided the original work is properly cited.

Abstract A standard practice used in the industry to discretizing the gravity term in the two-phase Darcy flow equations is to apply an upwind strategy. In this paper, we show that this can give a persistent unphysical flux field and an incorrect pressure distribution. As a solution to this problem, we present a new consistent discretization of flow, termed Gravitationally Consistent Multipoint Flux Approximation (GCMPFA), which is valid for both single- and two-phase flows. The discretization is based on the idea that the gravitational term in the flow equations is treated as part of the discrete flux operator and not as a right-hand side. Here, the traditional formulation representing pressure as a potential is extended to the case including gravity by introducing an additional set of right-hand side to the local linear system solved in the MPFA construction, thus obtaining an expression of the fluxes in terms of jumps in cell-center gravities. Numerical examples showing the convergence of the method are provided for both single- and two-phase flows. For two-phase flow, we show how our new method is capable of eliminating the unphysical fluxes arising when using a standard upwind scheme, thus converging to the correct pressure distribution.

1. Introduction

There exist several methods for solving numerically the single-phase and multiphase flow equations in porous media. Popular mass conservative schemes that can handle anisotropic permeability and/or grids that are not K-orthogonal include Mixed Finite Elements (Arbogast et al., 2007; Kim et al., 2007), Multipoint Flux Approximation (MPFA) (Aavatsmark, 2002; Aavatsmark et al., 1994, 1996, 1998a, 1998b, 2007, 2008; Edwards & Rogers, 1994, 1998; Edwards, 2000, 2002), and Multipoint Flux Mixed Finite Element (MFMFE) (Arrarás & Portero, 2019; Brezzi et al., 1985; Wheeler & Yotov, 2006; Wheeler et al., 2012) methods.

In this work, we discuss MPFA methods. MPFA is a control volume method introduced independently by two different research groups in 1994 (Aavatsmark et al., 1994; Edwards & Rogers, 1994). The two approaches differ on the choice of geometrical points and control volume grids. Here, we only consider the so-called O-method developed by Aavatsmark and coworkers. They first introduced MPFA for general quadrilateral grids in Aavatsmark et al. (1994) and Aavatsmark et al. (1996) and then extended the method to triangular and polygonal grids in Aavatsmark et al. (1998a, 1998b). The reader can refer to Aavatsmark (2002) for an excellent review on MPFA methods for quadrilateral grids and to Aavatsmark et al. (2007) for a numerical investigation on its convergence properties. The convergence properties of MPFA have also been investigated for general quadrilateral grids in Eigestad and Klausen (2005), Klausen and Winther (2006a), and Klausen and Winther (2006b) and for unstructured triangular grids in Bause et al. (2010). In particular, using a specific numerical quadrature, the MPFA and MFMFE methods were shown to be equivalent (Klausen & Winther, 2006a). A somewhat simpler MPFA variant is the so-called L-method by Aavatsmark et al. (2008). Finally, when the MPFA method is applied to multiphase flow, a monotone scheme is desirable. Local criteria which ensure monotonicity for general control volume methods on heterogeneous media are given in Nordbotten et al. (2007).

MFMFE methods were introduced for incompressible Darcy flow problems on triangular and convex quadrilaterals in Wheeler and Yotov (2006) using the lowest order Brezzi-Douglas-Marini spaces (Brezzi et al., 1985). Extensions to slightly compressible flow and multiphase flow are presented in Arrarás and Portero (2019) and Wheeler et al. (2012), respectively.

The common feature of all these methods is the treatment of the gravity term in the Darcy flow equations. The traditional approach has been to represent the pressure as a potential and let the discretization consider

only deviations from the potential, by ignoring gravity effects in the discretization. Gravity is only considered in the model equations in Arrarás and Portero (2019) and Wheeler et al. (2012), yet it is disregarded in the numerical examples reported therein.

However, this approach is inconsistent when the gravity term in the Darcy flow equation is inhomogeneous, as caused for example by two-phase effects, density variations, stepwise variations of permeability, and certain variants of vertically averaged models for CO_2 storage (Nordbotten & Celia, 2011). While for single-phase flow MPFA can handle discontinuities in the fluid potential caused by, for example, smooth variations of permeability from cell to cell, in two-phase flow discontinuities also arise due to presence and absence of a mobile phase, and this kind of discontinuities can create unphysical fluxes, for example, in the case of a fluid-fluid interface at conditions of vertical equilibrium (see Aavatsmark et al. (1994) for a discussion on this). Here, we show that a standard treatment of the gravity term based on an upwind strategy in the multiphase Darcy flow equations leads to the creation of a persistent unphysical flux field, even in absence of any external forces, and gives an incorrect pressure distribution.

An aim of this paper is therefore to develop a consistent discretization of the porous media flow equations in the presence of gravity which amends this crucial shortcoming. To do so, we treat the gravity term as part of the discrete flux operator and derive an expression of the fluxes in terms of jumps in cell-center gravities. The paper is organized as follows. First, we introduce the governing equations of single- and two-phase flow in porous media in section 2. Then, a standard discretization of the gravity term, and a discussion on its limitations, is presented in section 3. Our new consistent discretization of the flow equations in the presence of gravity is presented for single- and two-phase flow in sections 4 and 5, respectively. Numerical examples are provided in both sections. Finally, concluding remarks are given in section 6.

2. Governing Equations

2.1. Single-Phase Flow

Incompressible single-phase Darcy flow in nondeformable porous media is governed by the following equation:

$$\nabla \cdot [-\mathbf{K}(\nabla p + \mathbf{g})] = \psi, \tag{1}$$

where p is pressure, $\mathbf{K}$ is the (generally heterogeneous) absolute permeability tensor divided by fluid viscosity, $\mathbf{g}$ represents gravitational forces (density times acceleration due to gravity vector), which is a function of space, and ψ is a source term. We emphasize that equation (1) represents incorporation of Darcy's law into a mass conservation equation.

2.2. Two-Phase Flow

The Darcy formulation given by equation (1) is extended to incompressible immiscible two-phase flow as follows:

$$\phi \frac{\partial s_\alpha}{\partial t} - \nabla \cdot [\lambda_\alpha \mathbf{K}(\nabla p_\alpha + \mathbf{g}_\alpha)] = \psi_\alpha, \tag{2}$$

where ϕ is porosity, t is time, s_α is the phase saturation associated with phase $\alpha = 1, 2$, and λ_α is the phase mobility, which is an increasing function of s_α. In equation (2), $\mathbf{K}$ represents the absolute permeability tensor, as fluid viscosity is incorporated into λ_α. Introducing the total quantities $\zeta_\Sigma = \sum_\alpha \zeta_\alpha$, and in absence of capillary pressure, that is, $p_1 = p_2 = p$, summing equation (2) yields

$$-\nabla \cdot [\mathbf{K}(\lambda_\Sigma \nabla p + \mathbf{G}_\Sigma)] = \psi_\Sigma, \tag{3}$$

where $\mathbf{G}_\Sigma = \sum_\alpha (\lambda_\alpha \mathbf{g}_\alpha)$. The phase fluxes $\mathbf{q}_\alpha$ can then be expressed in terms of the total flux $\mathbf{q}_\Sigma$ through the fractional flow function $\varphi_\alpha = \lambda_\alpha / \lambda_\Sigma$ in the following manner:

$$\begin{aligned} \mathbf{q}_1 &= \varphi_1[\mathbf{q}_\Sigma + \lambda_2 \mathbf{K}(\mathbf{g}_2 - \mathbf{g}_1)], \\ \mathbf{q}_2 &= \varphi_2[\mathbf{q}_\Sigma - \lambda_1 \mathbf{K}(\mathbf{g}_2 - \mathbf{g}_1)]. \end{aligned} \tag{4}$$

Choosing one saturation as primary variable, say, for example, $s_2 = s$, equation (2) is reformulated in terms of total flux as

$$\phi \frac{\partial s}{\partial t} + \nabla \cdot \{\varphi_2[\mathbf{q}_\Sigma - \lambda_1 \mathbf{K}(\mathbf{g}_2 - \mathbf{g}_1)]\} = \psi_2. \tag{5}$$

Equations (3)–(5) form a system of two equations for two unknowns (s and p).

3. Standard Discretization of Flow

Solution of equation (1) using control volume methods involves the computation of the flux f_k through some surface ∂_k of the control volume, defined as

$$f_k = \int_{\partial_k} \mathbf{n} \cdot \mathbf{K}(\nabla p + \mathbf{g}) \mathrm{d}S, \tag{6}$$

where $\mathbf{n}$ is the unit normal vector to the surface. Likewise, for two-phase flow, from equation (3) one has the total flux

$$f_{\Sigma,k} = \int_{\partial_k} \mathbf{n} \cdot \mathbf{K}(\lambda_\Sigma \nabla p + \mathbf{G}_\Sigma) \mathrm{d}S. \tag{7}$$

3.1. Traditional Potential Formulation for Single-Phase Flow

Representing the pressure as a potential h, and ignoring gravity effects in the discretization, calculation of the flux in equation (6) reduces to the solution of the integral

$$f_k = \int_{\partial_k} \mathbf{n} \cdot \mathbf{K} \nabla h \mathrm{d}S. \tag{8}$$

3.1.1. One-Dimensional Problems

For one-dimensional problems, the flux over the surface between two neighbor cells 1 and 2, f_{12}, is approximated by a two-point stencil (see Figure 1 left) as follows:

$$f_{12} = T_{12}(h_1 - h_2), \tag{9}$$

where T_{12} is the transmissibility of the surface which is calculated as harmonic average of the cell transmissibilities, that is,

$$T_{12} = \frac{2}{T_1^{-1} + T_2^{-1}}. \tag{10}$$

The cell transmissibilities are defined as $T_i = K_i / \Delta x_i, i = 1, 2$, where Δx_i is the length of cell i.

3.1.2. Multidimensional Problems

For multidimensional problems, the flux is approximated using the MPFA method as

$$f_k = \int_{\partial_k} \mathbf{n} \cdot \mathbf{K} \nabla h \mathrm{d}S \approx \sum_i (t_{k,i} h_i), \tag{11}$$

where the coefficients $t_{k,i}$ are called transmissibility coefficients. Calculation of the transmissibility coefficients works as follows. A dual grid is created by connecting the cell centers with the face centers. In this manner, each cell is partitioned into subcells (three and four in triangular and quadrilateral grids and six and eight in tetrahedral and hexahedral grids, respectively) and each face is subdivided into subfaces (two in 2-D grids, four in 3-D grids). Subcells are then grouped together to form an interaction region surrounding each node (see Figure 1 right). Then, the following principles are applied:

1. Potential is assumed to be linear in each subcell.
2. Flux continuity is enforced at the subfaces.
3. Potential continuity is enforced at single points on the subfaces, called continuity points.

There is a whole class of MPFA methods for such grids, depending on the choice of the location of the continuity points. Here we only consider the O-method described by Aavatsmark (2002). Principles (1) and (3) imply that for a subface k with adjacent subcells j_1 and j_2, one has

$$h_{j_1} + \nabla h_{j_1} \cdot \mathbf{d}_{j_1 k} = h_{j_2} + \nabla h_{j_2} \cdot \mathbf{d}_{j_2 k}, \tag{12}$$

where ∇h is the subcell gradients and $\mathbf{d}$ is the distance between the continuity point and the cell centers. For flux continuity, principle (2) is written

$$\mathbf{n}_k \cdot \mathbf{K}_{j_1} \nabla h_{j_1} = \mathbf{n}_k \cdot \mathbf{K}_{j_2} \nabla h_{j_2}, \tag{13}$$

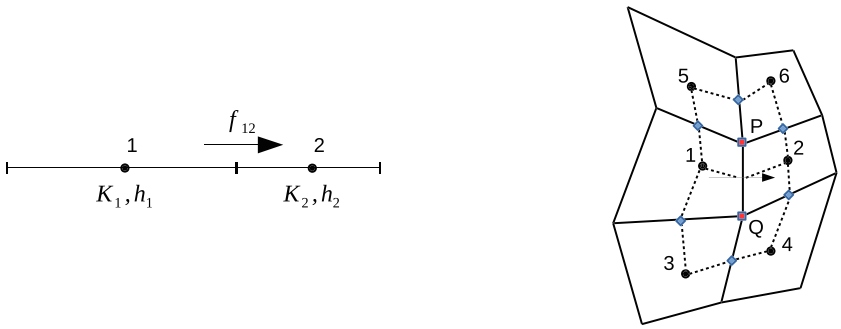

Figure 1. (left) One-dimensional (two points) stencil for flux calculation. (right) Multipoint stencil (six points) for calculation of flux f_{12}. Black circles are cell centers, red squares are interaction regions central points, and blue diamonds are continuity points, that is, face midpoints in the MPFA O-method. Calculation of the flux is done by summing the contributions from the two interaction regions (dashed lines) centered at points P and Q.

where $\mathbf{n}_k$ is the normal vector of the face and $\mathbf{K}_{j_i}$ is the permeability with respect to cells j_1 and j_2. Collecting all equations (12)–(13) for each interaction region, a local linear system is recovered of the following form:

$$\begin{bmatrix} \mathbf{G} & 0 \\ \mathbf{D} & \mathbf{I}_{\pm} \\ 0 & \mathbf{I} \end{bmatrix} \begin{bmatrix} \nabla h \\ h \end{bmatrix} = \begin{bmatrix} 0 \\ 0 \\ \mathbf{I} \end{bmatrix}. \tag{14}$$

The first row represents flux balance (13) and involves only the subcell potential gradients. The matrix $\mathbf{G}$ contains the discretized Darcy's law, that is, the $\mathbf{n}\cdot\mathbf{K}$ products on a subcell level. The second row gives pointwise potential continuity (12) over cell faces. Matrix $\mathbf{D}$ contains the distances $\mathbf{d}$, while matrix $\mathbf{I}_{\pm}$ contains ± 1 coefficients depending on which side the cell is relative to the face normal vector. The third row together with the right-hand side enforces a unit potential in one cell after another. Equation (14) can be inverted to compute the subcell potential gradients dh as functions of the cell-center potentials, effectively computing basis functions for the discretization. Hence, from solving equation (14) we obtain the transmissibility coefficients of the potential-to flux maps, denoted as $\omega_{k,i}$, which represent the contribution of cell i to the flux across the sub-face k. To obtain the full face coefficients $t_{k,i}$, we sum over the subfaces l of face k

$$t_{k,i} = \sum_l \omega_{l,i}. \tag{15}$$

The discretized flux across the face is then given by equation (11).

3.2. Standard Discretization of Single-Phase Flow

3.2.1. One-Dimensional Problems

In one-dimensional problems, we have seen that, in absence of gravity, the face transmissibility is calculated as harmonic average of the transmissibilities of the adjacent cells. If gravity is present, assuming that the pressure p is linear and gravitational forces g are constant within each cell, the flux continuity is given by

$$-K_1\left(\frac{\bar{p}-p_1}{\Delta x_1/2}+g_1\right) = -K_2\left(\frac{p_2-\bar{p}}{\Delta x_2/2}+g_2\right), \tag{16}$$

where $\bar{p}$ is the pressure at the interface between the two cells. Introducing the cell transmissibilities, equation (16) can be solved for $\bar{p}$ to get

$$\bar{p} = \frac{T_1 p_1 + T_2 p_2 + (T_2\Delta x_2 g_2 - T_1 \Delta x_1 g_1)/2}{T_1 + T_2}. \tag{17}$$

Inserting this expression back into, say, the left-hand side of equation (16) gives the flux expression in presence of gravity as

$$f_{12} = -\frac{2T_1T_2}{T_1+T_2}\left[(p_2-p_1)+\frac{\Delta x_1 g_1 + \Delta x_2 g_2}{2}\right] = T_{12}\left[(p_1-p_2)-\frac{\Delta x_1 g_1 + \Delta x_2 g_2}{2}\right]. \tag{18}$$

Equation (18) shows that for the pressure term the harmonic average of the cell transmissibilities is retrieved, whence the flux due to gravity is given by the product between the harmonic average of the cell transmissibilities times the arithmetic average of the cell gravitational forces.

3.2.2. Multidimensional Problems

Calculation of the full flux in the presence of gravity in equation (6) involves the computation of the term

$$g_k = \int_{\partial_k} \mathbf{n} \cdot \mathbf{K} \nabla \mathbf{g} \mathrm{d}S. \tag{19}$$

When this term is treated as a right-hand side in equation (1), a standard discretization approach is to extend the result of equation (18) to the multidimensional case and use the harmonic average of the cell permeability tensors. Defining $d_j = |\mathbf{x}_k - \mathbf{x}_j|$, the distance between the center of face k, $\mathbf{x}_k$, and the center of cell j, $\mathbf{x}_j$, where j is either of the two cells j_1 and j_2 with mutual face k, the flux due to gravity is then computed as

$$g_k \approx \mathbf{n}_k \cdot \langle \mathbf{K} \rangle_k \bar{\mathbf{g}}_k, \tag{20}$$

where the operator $\langle \mathbf{K} \rangle_k$ denotes the d-weighted harmonic average of the permeability tensors between the two cells j_1 and j_2

$$\langle \mathbf{K} \rangle_k = (d_{j_1} \mathbf{K}_{j_1}^{-1} + d_{j_2} \mathbf{K}_{j_2}^{-1})^{-1}, \tag{21}$$

and $\bar{\mathbf{g}}_k$ is the weighted arithmetic average of the cell gravity vectors

$$\bar{\mathbf{g}}_k = d_{j_1} \mathbf{g}_{j_1} + d_{j_2} \mathbf{g}_{j_2}. \tag{22}$$

The full flux in the presence of gravity is then given by

$$f_k \approx \sum_i (t_{k,i} p_i) + g_k, \tag{23}$$

where the transmissibilities coefficients $t_{k,i}$ are calculated as described in section 3.1.2.

3.3. Standard Discretization of Two-Phase Flow

3.3.1. Numerical Method

Solution of equations 3–(5) is done using the Implicit Pressure Explicit Saturation scheme (Chen et al., 2006). Starting from a known saturation s^n, the Implicit Pressure Explicit Saturation scheme works as follows:

1. The pressure p^n is calculated implicitly by solving (3) and the total flux $\mathbf{q}_\Sigma^n$ is reconstructed from p^n.
2. The saturation is advanced in time explicitly from (5) as

$$\phi \frac{s^{n+1} - s^n}{\Delta t} = -\nabla \cdot \{ \varphi_2^n [\mathbf{q}_\Sigma^n - \lambda_1^n \mathbf{K} (\mathbf{g}_2 - \mathbf{g}_1)] \} + \psi_2. \tag{24}$$

Calculation of the face mobilities in equation (24) is done using the method outlined in Moortgat et al. (2011). The method works as follows:

1. First, we pick the phase for which the phase flux has the same sign of the total flux. This is the heaviest phase when $(\mathbf{q}_\Sigma \cdot \mathbf{n})(\mathbf{K}\mathbf{g} \cdot \mathbf{n}) > 0$ or the lightest phase when $(\mathbf{q}_\Sigma \cdot \mathbf{n})(\mathbf{K}\mathbf{g} \cdot \mathbf{n}) < 0$. This sign determines the first upwind phase mobility λ_{α_1}.
2. For the other phase, we have two options. As a first guess, we assume that the second phase has the same sign as the first phase and the total flux and take the upwind mobility λ_{α_2} accordingly.
3. We can now evaluate the phase fluxes using equation (4) and check consistency. If the guessed sign is retrieved, then the process is complete, otherwise the opposite upwind choice for λ_{α_2} is made in step (2).

When the total flux is zero, the upwind directions can be determined explicitly. A standard discretization of the total flux in equation (7) is then obtained by applying the traditional MPFA construction to the pressure term and an upwind scheme to the gravity term as follows (Enchéry et al., 2002):

$$f_{\Sigma,k} \approx \lambda_{\Sigma,k} \sum_i (t_{k,i} p_i) + \mathbf{n}_k \cdot \langle \mathbf{K} \rangle_k (\lambda_{1,k} \mathbf{g}_1 + \lambda_{2,k} \mathbf{g}_2). \tag{25}$$

However, a discretization of such a kind on rough grids is prone to creating unphysical fluxes, as illustrated in the following section.

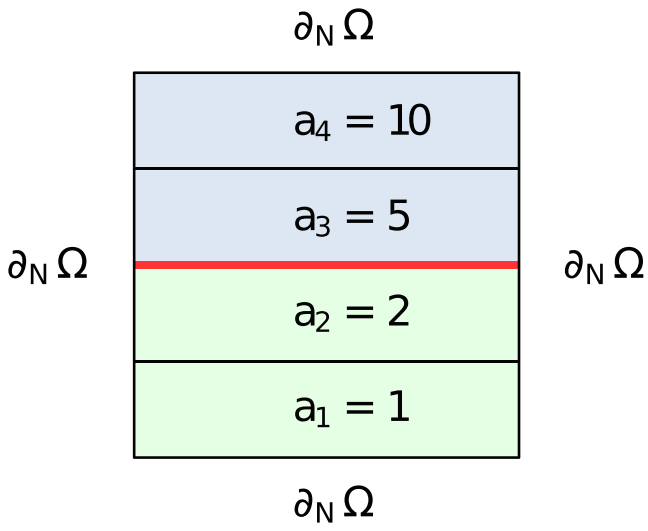

Figure 2. Initial and boundary conditions and values of permeability multiplier for test 3.3.2. In particular, no flow boundary conditions are assigned to all boundaries, that is, $q_\Sigma = q_1 = q_2 = 0$. Blue is the heaviest phase ($s_2 = 1$); green is the lightest phase ($s_2 = 0$).

3.3.2. Numerical Example

Let us consider the case of a system composed by two incompressible fluids trying to reach vertical equilibrium conditions in absence of any external forces. The two fluids have same viscosity equal to $1.0e^{-3}$ Pa·s, the gravity vector $\mathbf{g}$ is directed downward along the vertical direction, porosity ϕ is equal to 0.2, and the permeability tensor $\mathbf{K}$ is heterogenous with four layers of different permeabilities, that is, $\mathbf{K} = a_i K \mathbf{I}$, with $K = 1Da$ and values of a_i reported in Figure 2. No-flow boundary conditions are assigned to all boundaries, that is, $q_\Sigma = q_1 = q_2 = 0$. Initially, a horizontal interface is considered, with the upper region fully saturated with the heaviest phase ($\rho_2 = 1000$ kg/m^3) and the lower region fully saturated with the lightest phase ($\rho_1 = 100$ kg/m^3). Computations are carried out on quadrilateral randomly perturbed grids with five levels of refinement, that is, $N = 4, 8, 16, 32, 64$ number of cells per side. In virtue of equation (4), counter current flow between the two phases should thus establish, leading eventually to conditions of vertical equilibrium. However, numerical simulations using equation (25) indicate that a persistent spurious flux fields originate

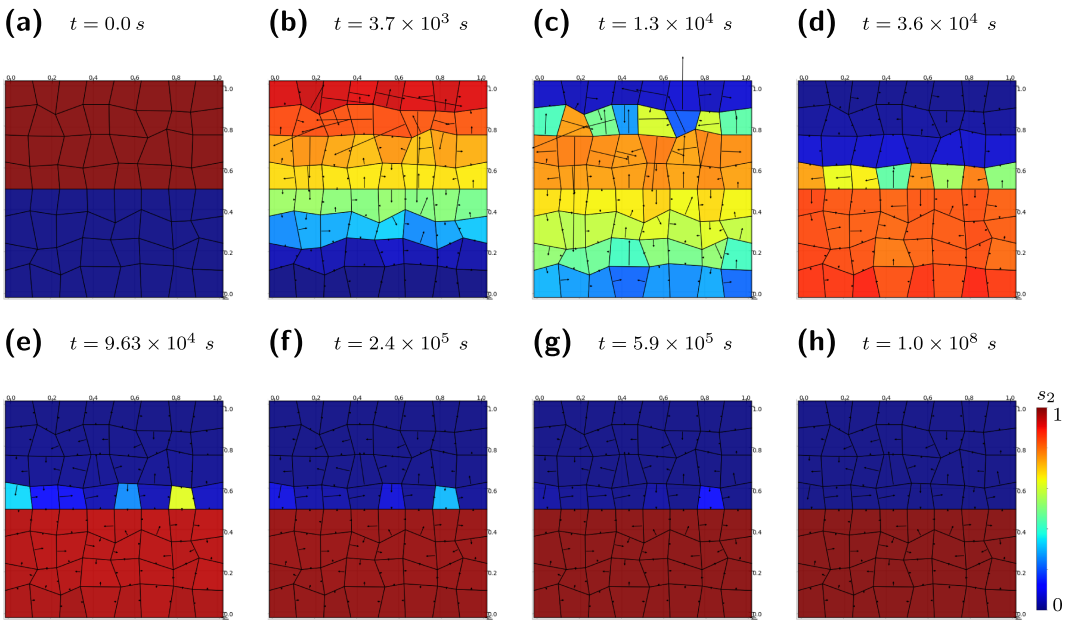

Figure 3. Time evolution of cell saturations of the heaviest phase and total fluxes at cell faces for test 3.3.2 with $N = 8$.

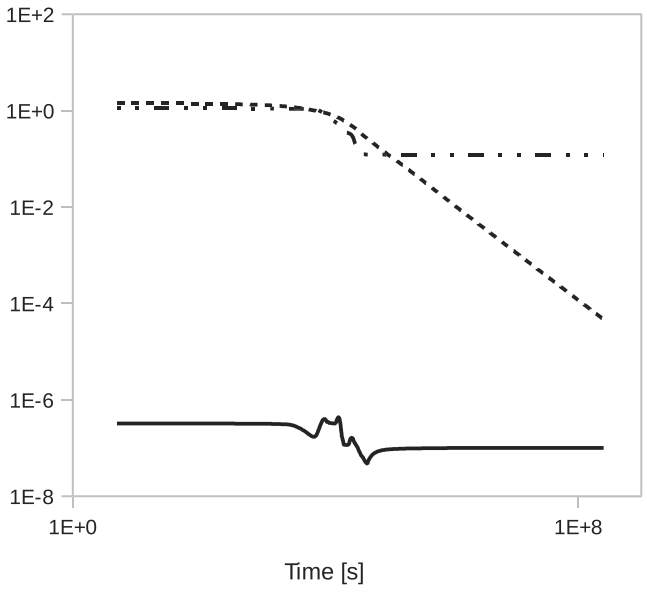

Figure 4. Errors in saturation and pressure and maximum total flux as a function of time for test 3.3.2 with $N = 8$. Continuous line: maximum total flux (with units of m/s). Dashed line: error in saturation. Dashed-dotted line: error in pressure.

(see Figure 3). After some oscillations, the system yet reaches a stable configuration; however, the computed pressure field is far from vertical equilibrium. This is clearly shown in Figure 4, displaying the time evolution of the errors in pressure and saturation and the maximum total flux. The errors in pressure and saturation are computed using the following L^2 metrics:

$$\varepsilon = \frac{\sqrt{\sum_i \Delta_i (\psi_i - \psi_{i,\text{exact}})^2}}{\sqrt{\sum_i \Delta_i \psi_{i,\text{exact}}^2}}, \tag{26}$$

where ψ is the computed variable, Δ is the element volume, and the exact variables are the ones measured at vertical equilibrium conditions. As Figure 4 clearly shows, the saturation converges to the equilibrium conditions; however, the nonvanishing total flux prevents the pressure to converge to vertical equilibrium conditions. This is because of the inconsistent discretization of the gravity term in the pressure equation, while a standard upwind scheme is sufficient for the transport equation. Nevertheless, the standard upwind scheme converges to the exact pressure field with refinement of the grid (first-order convergence; see Figure 5).

In the following sections, we present a consistent discretization of the flow equations in the presence of gravity, which is capable of eliminating this unphysical flux field and thus gives the correct pressure field.

4. Gravitationally Consistent Discretization of Single-Phase Flow

4.1. Numerical Method

For multidimensional problems, a consistent treatment of gravitational forces can be achieved by a more nuanced approach to the local flux balancing within the local construction of the discretization scheme. In the presence of a gravitational field, equation (13) is extended to read

$$\mathbf{n}_k \cdot \mathbf{K}_{j_1}(\nabla p_{j_1} + \mathbf{g}_{j_1}) = \mathbf{n}_k \cdot \mathbf{K}_{j_2}(\nabla p_{j_2} + \mathbf{g}_{j_2}), \tag{27}$$

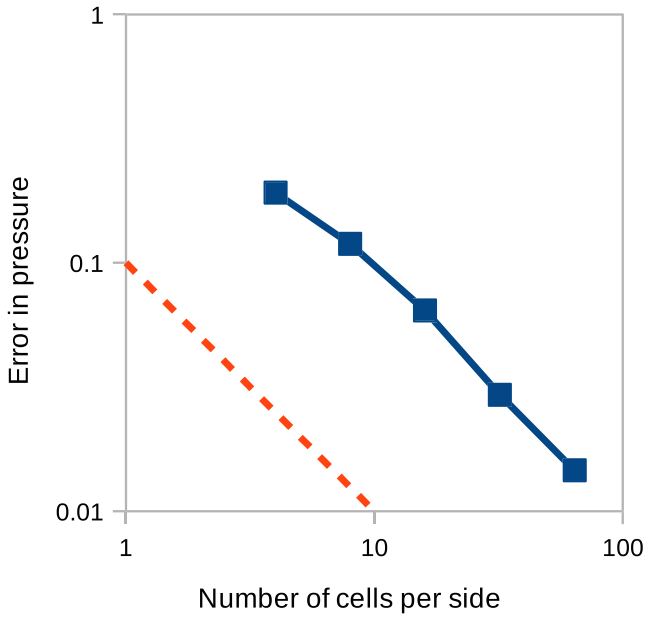

Figure 5. Convergence of pressure for test 3.3.2. Blue solid line: error in pressure. Red dashed line: linear convergence.

where $\mathbf{g}$ represents gravitational forces in the cells. We make the observation that jumps in the gravitational forces over the subfaces, $[[\mathbf{n}_k \cdot \mathbf{K}\mathbf{g}]]_k$, will act as a flux imbalance and thus induce an additional pressure gradient in the subcells. To extend the MPFA formulation to equation (27), we introduce an additional set of right-hand side functions, which applies nonzero conditions to the first row of (14). These additional right-hand side functions thus solve

$$\begin{bmatrix} \mathbf{G} & 0 \\ \mathbf{D} & \mathbf{I}_{\pm} \\ 0 & \mathbf{I} \end{bmatrix} \begin{bmatrix} dp \\ p \end{bmatrix} = \begin{bmatrix} \mathbf{I} \\ 0 \\ 0 \end{bmatrix}. \tag{28}$$

We now slightly reformulate equation (11) by considering $f_{k,j}$, which is the flux in absence of gravity across a subface k as evaluated in cell j (where j is either of the two cells j_1 and j_2 with mutual face k). The extended version of (11) is written for completeness as

$$f_{k,j} = \int_{\partial_k \Delta_j} \text{Tr}_{\partial_k \Delta_j} \mathbf{K} \nabla p \, dS \approx \sum_i (\omega_{k,j,i} p_i). \tag{29}$$

We make the note that the integral which is approximated is now stated slightly more precisely, in the sense that the integration volume Δ_j from which the boundary integral appears is explicit. Also, for the two cells j_1 and j_2 where $f_{k,j}$ is defined, it is clear from equation (14) that $f_{k,j_1} = f_{k,j_2}$

and therefore $\omega_{k,j_1,i} = \omega_{k,j_2,i} = \omega_{k,i}$. The transmissibility coefficients of the pressure-to-flux maps in absence of gravity, $\omega_{k,i}$, for the subface k, are then obtained by solving (14).

Similarly, let us denote the coefficients from (28) as $\nu_{k,j,l}$, which represent the flux across l due to a flux imbalance at k, as evaluated in cell j. We quickly note from equation (28) that for $l \neq k$, then as above $\nu_{k,j_1,i} = \nu_{k,j_2,i}$. However, this will not be the case for $k = l$, due to the flux imbalance, indeed in this case

$$\nu_{k,j_1,i} = -\nu_{k,j_2,i}. \tag{30}$$

We then obtain the full flux in the presence of gravity as

$$f_{k,j} = \int_{\partial_k \Delta_j} \mathrm{Tr}_{\partial_k \Delta_j} \mathbf{K}(\nabla p + \mathbf{g}) \mathrm{d}S \approx \sum_i (\omega_{k,j,i} p_i) + \sum_l (\nu_{k,j,l} [[\mathbf{n}_l \cdot \mathbf{K}\mathbf{g}]]_l) + |\partial_k| \mathbf{n}_k \cdot \mathbf{K}_j \mathbf{g}_j. \tag{31}$$

It is noted that due to equation (30), it follows that as expected $f_{k,j_1} = f_{k,j_2}$. Thus, the second subscript can be omitted as soon as a convention is chosen for what side the flux evaluation should be considered on. Therefore, one can make equation (31) symmetric by taking the mean of the two sides, that is,

$$f_k \approx \sum_i (\omega_{k,i} p_i) + \sum_i (\bar{\nu}_{k,l} [[\mathbf{n}_l \cdot \mathbf{K}\mathbf{g}]]_l) + \frac{1}{2} |\partial_k| \mathbf{n}_k \cdot (\mathbf{K}_{j_1} \mathbf{g}_{j_1} + \mathbf{K}_{j_2} \mathbf{g}_{j_2}), \tag{32}$$

where

$$\bar{\nu}_{k,l} = \frac{1}{2} (\nu_{k,j_1,l} + \nu_{k,j_2,l}). \tag{33}$$

Finally, we note that we can represent the $\mathbf{K}$-weighted jump operator over l in terms of vector coefficients $\check{\mu}_{l,j}$ as

$$[[\mathbf{n}_l \cdot \mathbf{K}\mathbf{g}]]_l = \sum_j \check{\mu}_{l,j} \cdot \mathbf{g}_j \tag{34}$$

and the mean of the cell gravities in terms of the coefficients $\bar{\mu}_{k,j}$ as

$$\frac{1}{2} |\partial_k| \mathbf{n}_k \cdot (\mathbf{K}_{j_1} \mathbf{g}_{j_1} + \mathbf{K}_{j_2} \mathbf{g}_{j_2}) = \sum_j \bar{\mu}_{k,j} \cdot \mathbf{g}_j. \tag{35}$$

With this in mind, we obtain the compound coefficients

$$\eta_{k,j} = \bar{\mu}_{k,j} + \sum_l \bar{\nu}_{k,l} \check{\mu}_{l,j}; \tag{36}$$

therefore, equation (32) can be written only in terms of cell-center sums as

$$f_k = \sum_i (\omega_{k,i} p_i + \eta_{k,i} \cdot \mathbf{g}_i). \tag{37}$$

We term this approach Gravitationally Consistent Multipoint Flux Approximation (GCMPFA).

4.2. Numerical Examples

4.2.1. Problem Formulation

In these examples, incompressible flow in a unit square domain is considered. The domain has a discontinuity line of equation $rx + sy = \delta$, where $0 \leq r, s, \delta \leq 1$ and $r + s = 1$. Gravitational forces are given as a linear combination of two contributions, namely, a step function across the discontinuity line $\mathbf{H}(x, y)$ which is normal to the discontinuity line, and a smooth function $\mathbf{P}(x, y)$, as follows:

$$\mathbf{g} = a_1 \mathbf{H}(x, y) + a_2 \mathbf{P}(x, y). \tag{38}$$

In the latter equation, a_1 and a_2 are two constants and, given the unit vectors $\mathbf{e}_x$ and $\mathbf{e}_y$, $\mathbf{H}(x, y)$ and $\mathbf{P}(x, y)$ have the following form:

$$\begin{aligned} \mathbf{H}(x, y) &= -\frac{h(x, y)}{\sqrt{r^2 + s^2}} (r\mathbf{e}_x + s\mathbf{e}_y), \\ \mathbf{P}(x, y) &= \cos(x)\cos(y)\mathbf{e}_x - \sin(x)\sin(y)\mathbf{e}_y, \end{aligned} \tag{39}$$

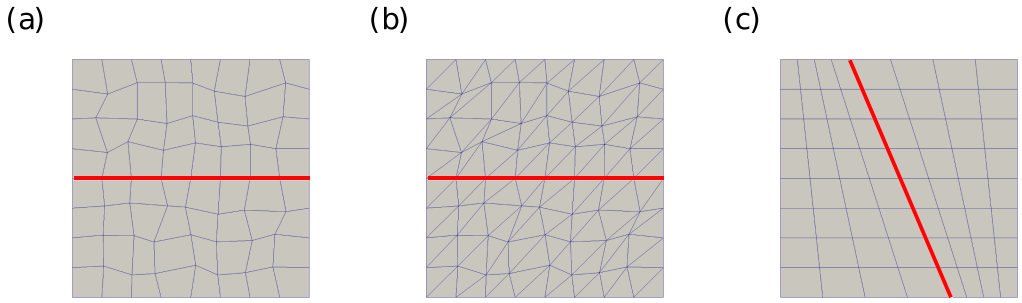

Figure 6. Grids used in the numerical tests, with discontinuity line in red.

with

$$h(x,y) = \begin{cases} h_1 & F > \delta \\ h_2 & F \leq \delta \end{cases}. \tag{40}$$

To test the convergence properties of the method, we choose an analytical solution such that

$$\mathbf{g} = -\nabla p, \tag{41}$$

so that zero normal flux conditions hold everywhere. The method is tested on different grids, namely, quadrilateral and triangular h-perturbed grids with horizontal discontinuity line ($r = 0$; see Figures 6a and 6b, respectively) and one regularly perturbed grid with an arbitrary discontinuity line ($r = 0.7$; see Figure 6c) $\delta = 0.5$ for all grids. Boundary conditions are of Neumann type at the top and bottom boundaries and of Dirichlet type at the left and right boundaries. Zero normal flux and pressure equal to the analytical solution are assigned to the respective boundaries. Finally, a unit homogeneous nondiagonal permeability tensor, with transverse component $K_t = 0.1$, is used.

To test the implementation, four cases are considered, depending on the values assigned to the coefficients a_i in equation (38) (see Table 1). In the first test, piecewise constant gravitational forces are considered ($a_2 = 0$). For this test, the GCMPFA method is expected to be exact. In the second test, there is no jump discontinuity, and gravitational forces are represented as a smooth field ($a_1 = 0$). Tests 3 and 4 have gravitational forces given by linear combination of $\mathbf{H}(x,y)$ and $\mathbf{P}(x,y)$ with different weighting coefficients. Finally, we make a comparison between our GCMPFA method given by equation (37) and the standard method given by equation (23).

4.2.2. Convergence Results

In the reported results, we consider errors using the following L^2 metrics

$$\varepsilon_p = \frac{\sqrt{\sum_i \Delta_i (p_i - p_{i,\text{exact}})^2}}{\sqrt{\sum_i \Delta_i p_{i,\text{exact}}^2}}, \tag{42}$$

$$\varepsilon_q = \sqrt{\sum_i \partial_{k,i}^2 (q_i - q_{i,\text{exact}})^2}. \tag{43}$$

For the convergence study, all simulations are run on a personal Desktop using Porepy (Keilegavlen et al., 2019), an open-source software framework for flow and transport in deformable fractured porous media

Table 1
Values of Weighting Coefficients Used in the Computations

Test	a_1	a_2
1	1	0
2	0	1
3	1	1
4	1	100

Table 2
Error ε_p on the Finest Grid (256 × 256) and Its Asymptotic Convergence Rate O_p, for All Tests and for Different Methods

	Quadrilaterals				Triangles				$r = 0.7$			
	GCMPFA		Standard		GCMPFA		Standard		GCMPFA		Standard	
Test	ε_p	O_p	ε_p	O_p	ε_p	O_p	ε_p	O_p	ε_p	O_p	ε_p	O_p
1	$1e^{-14}$	/	$1e^{-5}$	1.6	$2e^{-14}$	/	$2e^{-5}$	1.4	$3e^{-14}$	/	$2e^{-6}$	1.9
2	$7e^{-7}$	2.0	$7e^{-7}$	1.9	$5e^{-7}$	2.0	$5e^{-7}$	2.0	$9e^{-8}$	2.0	$1e^{-7}$	2.0
3	$2e^{-7}$	2.0	$1e^{-5}$	1.6	$1e^{-7}$	2.0	$2e^{-5}$	1.4	$8e^{-8}$	2.0	$2e^{-6}$	2.0
4	$2e^{-6}$	2.0	$2e^{-6}$	2.1	$1e^{-6}$	2.0	$2e^{-6}$	1.9	$2e^{-6}$	2.0	$2e^{-6}$	2.0

developed within the Porous Media Group at the Department of Mathematics, University of Bergen. The full study contains 4×3×7×2 = 168 computations, the results of which are summarized in Tables 2 and 3. Table 2 shows the results for the error ε_p and its asymptotic convergence rate O_p, while Table 3 shows the results for the error ε_q and its asymptotic convergence rate O_q. As expected, when gravitational forces are piecewise constant (Test 1), the GCMPFA method is exact to working precision for both pressure and fluxes, while a standard treatment of the gravity term leads to a discretization error. We remark that the two approaches coincide if the grid is K-orthogonal. It is also noted that for this test, the convergence rate for pressure of the standard method for the h-perturbed grids is generally worse than the second order usually obtained using traditional MPFA methods without gravity. The standard method recovers second-order convergence for Test 2. In this case, the two methods behave similarly. The superiority of the GCMPFA method over the standard method is clearly highlighted when the gravity field is a smooth discontinuous function (Tests 3 and 4). In this case, the GCMPFA method always retains second-order convergence for both pressure and fluxes, independently of the magnitude of the weighting coefficients a_i. Conversely, the standard method always shows a reduction in convergence rate for fluxes O_q to 1.5 and only achieves second-order convergence for pressure when the magnitude of the smooth part is much greater than that of the discontinuous part, that is, when $a_2 \gg a_1$ (Test 4). We summarize the results of Tables 2 and 3 heuristically as follows.

• For h-perturbed grids, the GCMPFA method exhibits a numerical convergence following

$$O_p = O_q = a_2 h^2. \tag{44}$$

• For h-perturbed grids, the standard method exhibits a numerical convergence following

$$\begin{aligned} O_p &= a_1 h^{1.5} + a_2 h^2, \\ O_q &= a_1 h^{1.5} + \tau a_2 h^2, \end{aligned} \tag{45}$$

where τ is equal to 1 if $a_1 = 0$ and is equal to 0 otherwise.

We remark that the results presented in equations (44) and (45) are based solely on the tests considered here, as the framework for proving convergence of MPFA methods without assuming smoothness of the permeability coefficient typically does not yield convergence rates, since a priori knowledge of the regularity of the solution cannot be assumed (Agelas & Masson, 2008).

Table 3
Error ε_q on the Finest Grid (256 × 256), and Its Asymptotic Convergence Rate O_q, for All Tests and for Different Methods

	Quadrilaterals				Triangles				$r = 0.7$			
	GCMPFA		Standard		GCMPFA		Standard		GCMPFA		Standard	
Test	ε_q	O_q	ε_q	O_q	ε_q	O_q	ε_q	O_q	ε_q	O_q	ε_q	O_q
1	$5e^{-15}$	/	$1e^{-4}$	1.4	$1e^{-14}$	/	$3e^{-4}$	1.6	$1e^{-14}$	/	$4e^{-4}$	1.5
2	$3e^{-7}$	2.0	$3e^{-7}$	2.0	$1e^{-7}$	2.0	$3e^{-7}$	2.0	$4e^{-9}$	3.0	$6e^{-8}$	2.5
3	$3e^{-7}$	2.0	$1e^{-4}$	1.4	$1e^{-7}$	2.0	$3e^{-4}$	1.6	$4e^{-9}$	3.0	$4e^{-4}$	1.5
4	$3e^{-5}$	2.0	$1e^{-4}$	1.5	$1e^{-5}$	2.0	$3e^{-4}$	1.6	$4e^{-7}$	3.0	$4e^{-4}$	1.5

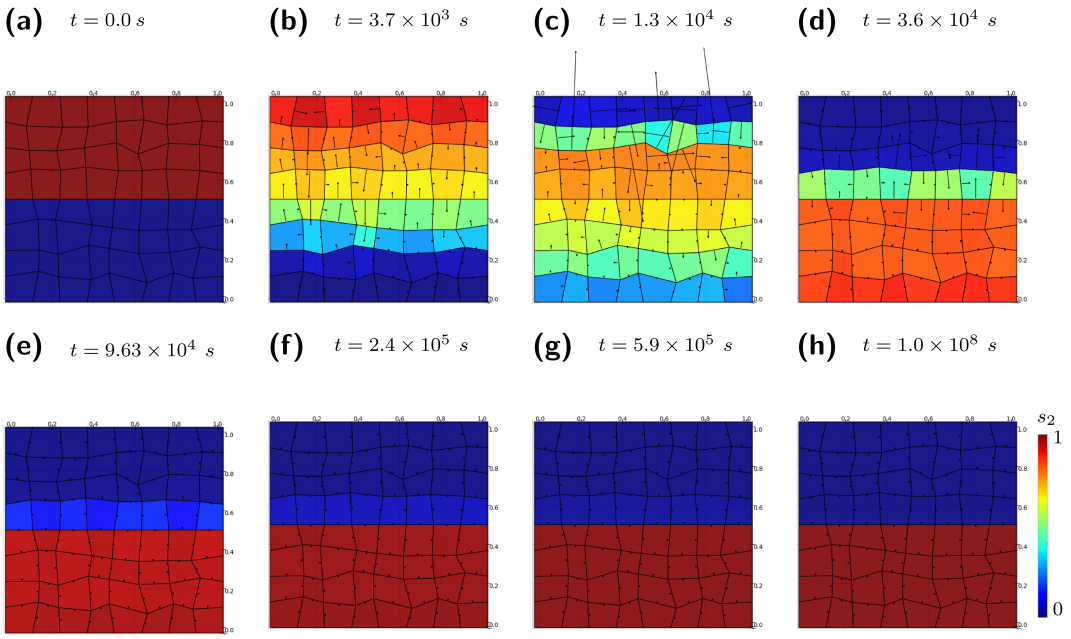

Figure 7. Time evolution of cell saturations of the heaviest phase and total fluxes at cell faces obtained with the GCMPFA method for test 5.2 with $N = 8$.

5. Gravitationally Consistent Discretization of Two-Phase Flow

5.1. Numerical Method

A consistent discretization of the gravity term for two-phase flow is done by extending the flux formulation given by equation (31) to the total flux in the following manner:

$$f_{\Sigma,k} \approx \sum_i (\omega_{\Sigma,k,i} p_i) + \sum_l (\nu_{k,j,l} [[\mathbf{n}_l \cdot \mathbf{K}\mathbf{G}_\Sigma]]_l) + |\partial_k| \mathbf{n}_k \cdot \mathbf{K}_j \mathbf{G}_{\Sigma,j}. \tag{46}$$

In terms of cell-center sums only, equation (46) is written

$$f_{\Sigma,k} = \sum_i (\omega_{\Sigma,k,i} p_i + \eta_{k,i} \cdot \mathbf{g}_i), \tag{47}$$

which is the two-phase counterpart of equation (37). The remaining part of the algorithm works as illustrated in section 3.3.1.

5.2. Numerical Example

We consider the same example of section 3.3.2, and we test whether the new GCMPFA discretization given by equation (47) is capable of eliminating the spurious flux field arising when using the standard upwind method given by equation (25). Figure 7 shows the time evolution of the cell saturations of the heaviest phase obtained using the GCMPFA method. Comparing Figure 7 to the same figure obtained using the stadard upwind method (see Figure 3), two things can be noted. First, the spurious flux field vanishes once the two fluids approach their equlibrium configuration, that is, for $t > 1 \times 10^5\ s$ (subfigure (e) onward). Second, countercurrent flow is more uniformly distributed, that is, no oscillating saturations are observed at the near-interface region (compare subfigures (d)–(g)). Figure 8 shows the errors in saturation and pressure and the maximum total flux as a function of time for the two methods for $N = 64$. As the figure clearly shows, as opposite to the standard method, the GCMPFA method is capable of eliminating the spurious flux field (see Figure 8c), and thus, the pressure converges to conditions of vertical equilibrium (see Figure 8b). The saturation is not substantially affected by the different solution methods for the pressure equation; however, it shows faster convergence with the GCMPFA method (see Figure 8a).

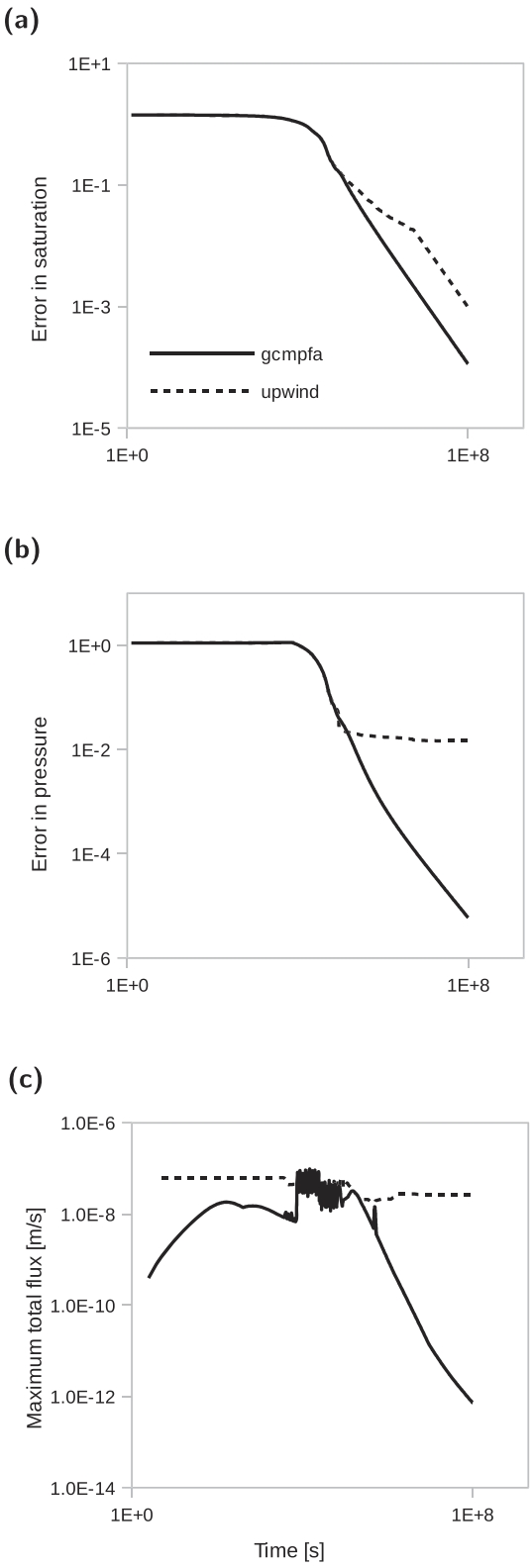

Figure 8. Error in saturation (a), error in pressure (b), and maximum total flux (c) as a function of time for the two methods for test 5.2 with $N = 64$.

6. Conclusions

We presented a novel consistent discretization of flow for inhomogeneous gravitational fields, valid for both single- and two-phase flows. The discretization is based on the idea that the gravity term is treated as part of the discrete flux operator and not as a right-hand side. This is achieved by introducing an additional set of right-hand side to the local linear system solved in the MPFA construction, thus obtaining an expression of the fluxes in terms of jumps in cell-center gravities. We provided numerical examples showing the convergence of the method. For single-phase flow, the examples indicate that for rough grids we have a general second-order convergence of the scheme in terms of both pressure and fluxes. This is in contrast to the standard discretization approach for the gravity term using the harmonic average of the cell permeability tensors. For this latter discretization, second-order convergence is reduced when the gravity undergoes stepwise variations from cell to cell. Finally, we provided numerical evidence that, in contrast to the standard upwind strategy used in the industry, the GCMPFA is capable of equilibrating a system of two incompressible fluids in absence of any external forces. This is particularly useful in reservoir simulations applications when vertical equilibrium conditions are sought as initial conditions. We conclude by remarking that, although the numerical examples presented here are two-dimensional, our method is general to multidimensional problems. Besides, extension to three-phase models is straightforward. Extensions to other variants of MPFA methods (such as the L-method) or to slightly compressible flow are also possible, but they are not addressed here.

Acknowledgments
This work forms part of Norwegian Research Council Project 250223. Data are available online (https://doi.org/10.5281/zenodo.3413545.).

References

Aavatsmark, I. (2002). An introduction to multipoint flux approximations for quadrilateral grids. *Computational Geosciences*, *6*(3-4), 405–432.

Aavatsmark, I., Barkve, T., Bøe, Ø., & Mannseth, T. (1994). Discretization on non-orthogonal, curvilinear grids for multi-phase flow. In *Ecmor iv-4th european conference on the mathematics of oil recovery*.

Aavatsmark, Ivar, Barkve, T., Bøe, Ø., & Mannseth, T. (1996). Discretization on non-orthogonal, quadrilateral grids for inhomogeneous, anisotropic media. *Journal of computational physics*, *127*(1), 2–14.

Aavatsmark, I., Barkve, T., Bøe, O, & Mannseth, T. (1998a). Discretization on unstructured grids for inhomogeneous, anisotropic media. part i: Derivation of the methods. *SIAM Journal on Scientific Computing*, *19*(5), 1700–1716.

Aavatsmark, I., Barkve, T., Bøe, O, & Mannseth, T. (1998b). Discretization on unstructured grids for inhomogeneous, anisotropic media. part II: Discussion and numerical results. *SIAM Journal on Scientific Computing*, *19*(5), 1717–1736.

Aavatsmark, I., Eigestad, G. T., Klausen, R. A., Wheeler, M. F., & Yotov, I. (2007). Convergence of a symmetric MPFA method on quadrilateral grids. *Computational Geosciences*, *11*(4), 333–345.

Aavatsmark, I., Eigestad, G. T., Mallison, B. T., & Nordbotten, J. M. (2008). A compact multipoint flux approximation method with improved robustness. *Numerical Methods for Partial Differential Equations: An International Journal*, *24*(5), 1329–1360.

Agelas, L., & Masson, R. (2008). Convergence of the finite volume MPFA O scheme for heterogeneous anisotropic diffusion problems on general meshes. *Comptes rendus de l'Académie des Sciences*, *346*, 1007–1012.

Arbogast, T., Pencheva, G., Wheeler, M. F., & Yotov, I. (2007). A multiscale mortar mixed finite element method. *Multiscale Modeling & Simulation*, *6*(1), 319–346.

Arrarás, A., & Portero, L. (2019). Multipoint flux mixed finite element methods for slightly compressible flow in porous media. *Computers & Mathematics with Applications*, *77*(6), 1437–1452.

Bause, M., Hoffmann, J., & Knabner, P. (2010). First-order convergence of multi-point flux approximation on triangular grids and comparison with mixed finite element methods. *Numerische Mathematik*, *116*(1), 1–29.

Brezzi, F., Douglas, J., & Marini, L. D. (1985). Two families of mixed finite elements for second order elliptic problems. *Numerische Mathematik*, *47*(2), 217–235.

Chen, Z., Huan, G., & Ma, Y. (2006). Computational methods for multiphase flows in porous media (Vol. *2*). SIAM.

Edwards, M. G. (2000). M-matrix flux splitting for general full tensor discretization operators on structured and unstructured grids. *Journal of Computational Physics*, *160*(1), 1–28.

Edwards, M. G. (2002). Unstructured, control-volume distributed, full-tensor finite-volume schemes with flow based grids. *Computational Geosciences*, *6*(3-4), 433–452.

Edwards, M. G., & Rogers, C. F. (1994). A flux continuous scheme for the full tensor pressure equation. In *Ecmor iv-4th european conference on the mathematics of oil recovery*.

Edwards, M. G., & Rogers, C. F. (1998). Finite volume discretization with imposed flux continuity for the general tensor pressure equation. *Computational geosciences*, *2*(4), 259–290.

Eigestad, G. T., & Klausen, R. A. (2005). On the convergence of the multi-point flux approximation O-method: Numerical experiments for discontinuous permeability. *Numerical Methods for Partial Differential Equations: An International Journal*, *21*(6), 1079–1098.

Enchéry, G, Masson, R., Wolf, S., & Eymard, R. (2002). Mathematical and numerical study of an industrial scheme for two-phase flows in porous media under gravity. *Computational Methods in Applied Mathematics*, *2*(4), 325–353.

Keilegavlen, E., Berge, R., Fumagalli, A., Starnoni, M., Stefansson, I., Varela, J., & Berre, I. (2019). Porepy: An open-source software for simulation of multiphysics processes in fractured porous media. arXiv preprint arXiv:1908.09869.

Kim, M.-Y., Park, E.-J., Thomas, S. G., & Wheeler, M. F. (2007). A multiscale mortar mixed finite element method for slightly compressible flows in porous media. *Journal of the Korean Mathematical Society*, *44*(5), 1103–1119.

Klausen, R. A., & Winther, R. (2006a). Convergence of multipoint flux approximations on quadrilateral grids. *Numerical Methods for Partial Differential Equations: An International Journal*, *22*(6), 1438–1454.

Klausen, R. A., & Winther, R. (2006b). Robust convergence of multi point flux approximation on rough grids. *Numerische Mathematik*, *104*(3), 317–337.

Moortgat, J., Sun, S., & Firoozabadi, A. (2011). Compositional modeling of three-phase flow with gravity using higher-order finite element methods. *Water Resources Research*, *47*(5).

Nordbotten, J. M., Aavatsmark, I., & Eigestad, G. T. (2007). Monotonicity of control volume methods. *Numerische Mathematik*, *106*(2), 255–288.

Nordbotten, J. M., & Celia, M. A. (2011). *Geological Storage of CO_2: Modeling Approaches for Large-Scale Simulation*. John Wiley & Sons.

Wheeler, M. F., Xue, G., & Yotov, I. (2012). Accurate cell-centered discretizations for modeling multiphase flow in porous media on general hexahedral and simplicial grids. *SPE Journal*, *17*(03), 779–793.

Wheeler, M. F, & Yotov, I. (2006). A multipoint flux mixed finite element method. *SIAM Journal on Numerical Analysis*, *44*(5), 2082–2106.